

Aharonov-Bohm caging of an electron in a quantum fractal

Biplab Pal*

Department of Physics, School of Sciences, Nagaland University, Lumami-798627, Nagaland, India

(Dated: June 7, 2025)

Fractal geometries exhibit complex structures with scale invariance self-similar pattern over various length scales. An artificially designed quantum fractal geometry embedded in a uniform magnetic flux has been explored in this study. It has been found that due to quantum mechanical effect, such quantum fractal display an exotic electronic property which is reflected in its transport characteristics. Owing to this uniform magnetic flux piercing through each closed-loop building block of the fractal structure, an electron traversing through such a fractal geometry will pick up a nontrivial Aharonov-Bohm phase factor, which will influence its transport through the system. It is shown that, one can completely block the transmission of an electron in this fractal geometry by setting the value of the uniform magnetic flux to half flux quantum. This phenomenon of Aharonov-Bohm caging of an electron in this quantum fractal geometry has been supported by the computation of the energy spectrum, two-terminal transport and persistent current in its various generations. This result is very robust against disorder and could be useful in designing efficient quantum algorithms using a quantum fractal network.

Keywords: Fractal; Aharonov-Bohm caging; Tight-binding model; Quantum transport; Persistent current

I. INTRODUCTION

The lattice geometry and quantum mechanical effects play a pivotal role in controlling the quantum transport properties in low-dimensional quantum systems. The quantum transport property of a quantum system render a very significant role in processing the quantum information in the system as well as for building efficient quantum algorithms. The nature of the electronic states in the system, *i.e.*, whether they are localized or extended, greatly influences the quantum transport properties of the system. For example, with any arbitrary amount of disorder in one- and two-dimensional quantum systems, all the single-particle states exhibit the well-known phenomena of Anderson localization [1, 2], where all the single-particle states are exponentially localized making the system to act as an insulator with zero transport. However, we can also have situations where one can have complete localization of an electronic state in absence of any disorder in the system. Such disorder-free localization of electronic states happens purely because of the underlying lattice topology [3] and the destructive quantum interferences of the wavefunction. This phenomenon has led to a very exciting area of research known as the flat-band localization [4, 5].

Interestingly, one of the prototype sub-category examples of such flat-band localization for certain lattice geometries can emerge even in presence of an external magnetic flux in the system [6–9, 12]. The origin of this phenomenon lies in some fundamental aspects of quantum mechanics, where a charge particle moving around a closed-loop geometry pierced by a nonzero magnetic flux, picks up a geometric phase factor in its wavefunction known as the Aharonov-Bohm phase [13]. For certain

specific lattice geometries, such as one-dimensional (1D) diamond lattice [9–11] and two-dimensional (2D) \mathcal{T}_3 lattice [12], we encounter a very special situation where the single-particle energy spectrum collapses to a few points for certain special value of the underlying magnetic flux equal to half flux quantum. This phenomenon is called as the Aharonov-Bohm (AB) caging, where all the single-particle states in the system are highly localized giving rise to zero transport. In recent times, this remarkable quantum effect has drawn a prevailing research attention and has been experimentally realized with the state-of-art ultrafast laser-writing technology in photonics using a synthetic magnetic flux [14, 15] and also in optical lattice of ultracold atoms with tailored gauge fields [16]. Lately, the idea of AB caging has also been extended for a variety of decorated lattice geometries in the context of topological insulator in lattice models [17–19].

As of now, the AB caging phenomena has been realized for lattices with integer dimensions, such as in 1D and 2D lattices. An intriguing question one can ask is that, can we capture this exotic phenomena in a lattice geometry with fractional dimension? We address this issue in this research article and show that it is indeed possible to realize the AB caging in a lattice geometry with *fractional* dimension. In a fractal lattice, as it grows in size, we start to have more and more holes appearing in its structure and hence it offers *fractional* dimension. This makes fractal lattices very interesting and in recent times, it has generated a keen interest in the scientific community from various aspects, namely, topological phases of matter [20–23], quantum Hall effect [24–26], flatband physics [27–32], Bose-Einstein condensates [33], Josephson effect [34] etc., are to name a few among others. One of the recent exciting developments is that, these complex fractal structures are not just anymore mere theoretical artifact, but they have been synthesized in real-life experiments in the laboratory using various advanced technologies, such as self-assembly molecular growth techniques [35, 36],

* E-mail: biplab@nagalanduniversity.ac.in

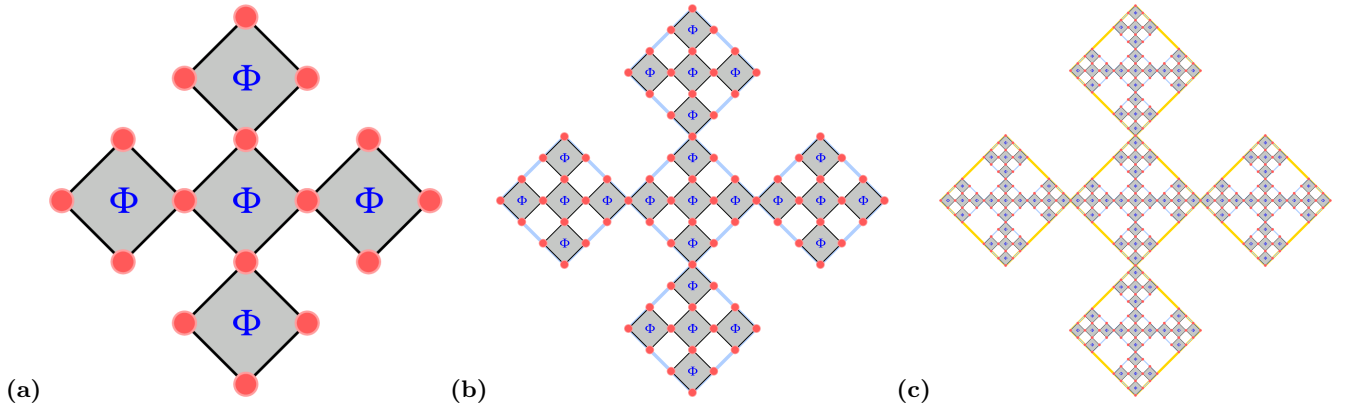


FIG. 1. Schematic diagram of various generations, *viz.*, (a) first generation (\mathcal{G}_1), (b) second generation (\mathcal{G}_2), and (c) third generation (\mathcal{G}_3) of a closed-loop Vicsek fractal lattice geometry with all the diamond-shaped closed-loop building blocks pierced by a nonzero uniform magnetic flux Φ .

atomic manipulation method with scanning tunnelling microscope [37, 38], and femtosecond laser-writing technique [29–31]. These experimental advances in the fractal growth techniques encourage us to theoretically investigate the AB caging phenomena in a quantum fractal geometry [39].

In this study, we have considered a fractal lattice geometry built out of diamond-shaped building blocks which is popularly known as the *Vicsek* snowflake or *Vicsek* fractal [40–44] with the Hausdorff dimension $d_f = \log(5)/\log(3) \approx 1.465$. Such fractal geometry is not only important from the point view of physics, but also it is found to be very useful in the field of aerospace engineering [40], mathematics [41], random walk statistics [42], and so on. In our model, all the diamond-shaped closed-loop plaquettes are penetrated by a nonzero uniform magnetic flux as depicted in Fig. 1. Due to the quantum mechanical effect, this will induce a geometric phase factor known as the AB phase in the wavefunction of the electron, when it will traverse through this lattice structure. We have shown that, for a special value of the magnetic flux, one can completely block the transmission of the electron in this fractal system. Thus, we encounter the phenomenon of AB caging in such a quantum fractal geometry. We quantify this result by a rigorous computation of the energy spectrum, density of states, two-terminal transport characteristics, and persistent current upto the third generation Vicsek fractal geometry. We have also verified that the phenomenon of AB caging in this fractal geometry is very robust against the onsite disorder in the system.

Our findings and analysis are presented in the following. The structure of the article is as follows: In Sec. II, we define the tight-binding Hamiltonian which describe our lattice model, and show the results for the energy eigenvalue spectrum as a function of the magnetic flux for this fractal lattice geometry in its various generations. Sec. III deals with the results and analysis for the density of states and the two-terminal transport properties of the system with different values of the magnetic flux upto

the third generation Vicsek fractal geometry, alongwith a brief discussion on the effect of onsite disorder on the AB caging phenomenon for this fractal system. The results for the persistent current in this closed-loop fractal geometry is presented in the Sec. IV. Finally, in Sec. V, we draw our conclusion by summarizing the central result of this study and possible future scope.

II. THE HAMILTONIAN AND THE ENERGY SPECTRUM

The single-particle states in a Vicsek fractal lattice as shown in Fig. 1 can be mathematically described by the following tight-binding Hamiltonian:

$$\mathbf{H} = \sum_n \varepsilon_n c_n^\dagger c_n + \sum_{\langle n,m \rangle} (t_{nm} e^{i\theta_{nm}} c_m^\dagger c_n + \text{h.c.}), \quad (1)$$

where the first term represents the potential energy term and the second term represents the kinetic energy term. In the language of tight-binding formalism, ε_n is known as the onsite potential at the n th site and t_{nm} is known as the nearest-neighbor hopping integral between the two neighboring sites ' n ' and ' m ' in the fractal lattice geometry. c_n^\dagger (c_n) are the operators which creates (annihilates) a single-particle state at the n th site. $\theta_{nm} = \frac{2\pi\Phi}{4\Phi_0}$ is the AB phase acquired by the electron wavefunction while hopping from the n th site to m th site along a diamond-shaped loop in the clockwise direction as a effect of the enclosed magnetic flux Φ (measured in units of the fundamental flux quantum $\Phi_0 = h/e$). The dimension of the Hamiltonian for the system is governed by the total number of sites in the Vicsek fractal lattice geometry in a given generation \mathcal{G}_ℓ following the prescription given by

$$\mathcal{N}_\ell = [3R^\ell + 1], \quad (2)$$

where $R = 5$ is the repetition factor for the Vicsek fractal geometry and ' ℓ ' represents the generation index.

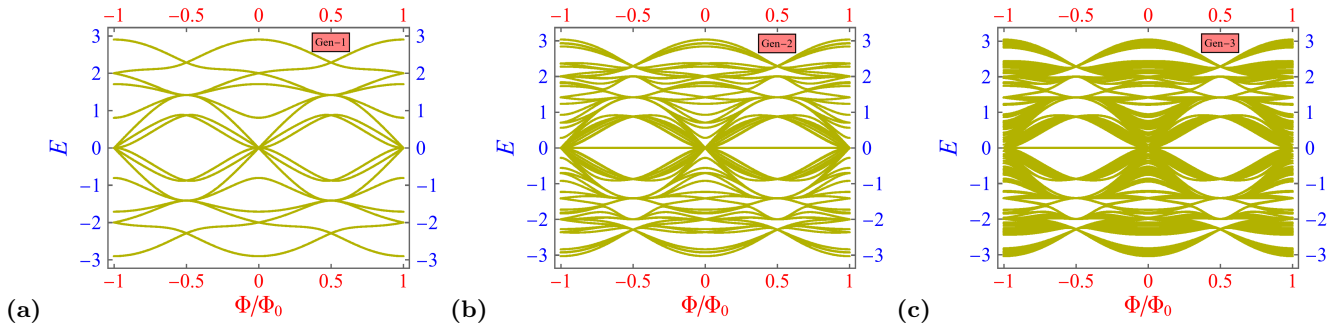


FIG. 2. Variation in the energy eigenvalue spectrum (E) as function of the Aharonov-Bohm flux (Φ) for (a) first generation (with $\mathcal{N}_1 = 16$ sites), (b) second generation (with $\mathcal{N}_2 = 76$ sites), and (c) third generation (with $\mathcal{N}_3 = 376$ sites) Vicsek fractal lattice structure, respectively. We set the onsite potential $\varepsilon_n = 0$ for all n -sites and the nearest-neighbor hopping integral $t_{nm} = t = 1$ for all $\langle n, m \rangle$ bonds.

All the important information and properties of the Vicsek fractal system can be extracted from the Hamiltonian of the system. At first, we focus on the energy eigenvalues spectrum of the Vicsek fractal system. One can easily obtain the energy eigenvalue spectrum for any ℓ th generation Vicsek fractal geometry by diagonalizing the corresponding ($\mathcal{N}_\ell \times \mathcal{N}_\ell$) Hamiltonian matrix for the system. We have done this upto the third generation Vicsek fractal lattice and shown the variation in the energy eigenvalue spectrum for the system as a function of the uniform Aharonov-Bohm flux Φ (see Fig. 2). The Aharonov-Bohm flux Φ has a periodicity 0 to Φ_0 (the fundamental flux quantum), which is clearly reflected from the energy eigenvalue pattern displayed in Fig. 2. The energy eigenvalues E are measured in units of the hopping integral t . One of the fundamental features of any fractal system is that, it has an inherent self-similar character in it, which is also emulated in the energy spectrum shown in Fig. 2(a)-(c). As the fractal generation increases, the number of lattice sites in the system also increases. Hence, the energy spectrum also become more and more denser, and after a certain generation it reaches the saturation value where one cannot distinguish the spectrum from its previous generation.

If we scan through the x -axis in the Fig. 2(a)-(c), we can identify a very interesting thing happening at the value $\Phi = \pm\Phi_0/2$ — at this particular value of the magnetic flux, the energy spectrum shrink to a few points. This is a clear indication of the fact that, at this particular value of the magnetic flux, the single-particle states in this fractal lattice model are highly localized giving rise to the AB caging phenomena in a quantum fractal system. Another interesting observation is that, starting from the second generation fractal lattice onward, the eigenvalue at $E = 0$ emerges in the spectrum (see Fig. 2(b)), which is not there in the spectrum for the first generation fractal system (see Fig. 2(a)). The possible reason behind the appearance of this feature is that the eigenvalue at $E = 0$ acts like an edge or corner state for this particular fractal lattice geometry. As we go the second generation Vicsek fractal system (see Fig. 1(b)),

the holes in the system becomes more prominent, clearly distinguishing the notion of the edge or corner in the fractal system. It is to be noted that, the $E = 0$ state is very robust against the variation of the magnetic flux in the system. In Sec. III, we substantiate the results and analysis presented in this section through a rigorous computation of the density of states and the two-terminal transport properties for this fractal lattice model.

III. THE DENSITY OF STATES AND THE TRANSPORT CHARACTERISTICS

The density of states (DOS) of a tight-binding lattice model gives us an indication about the character of the single-particle eigenfunctions in the system, *i.e.*, whether they are extended or localized. We use the Green's function formalism to evaluate the DOS for such closed-loop fractal structures [45–47]. The DOS in terms of the Green's function $\mathbf{G}(E, \Phi)$ of the system is given by

$$\mathfrak{D}(E, \Phi) = -\frac{1}{\pi\mathcal{N}_\ell} \text{Im} \left[\text{Tr} [\mathbf{G}(E, \Phi)] \right], \quad (3)$$

where $\mathbf{G}(E, \Phi) = [(E + i\eta)\mathbf{I} - \mathbf{H}]^{-1}$ (with $\eta \rightarrow 0^+$), \mathbf{I} is an Identity matrix of dimension ($\mathcal{N}_\ell \times \mathcal{N}_\ell$), \mathcal{N}_ℓ is the number of sites in an ℓ th generation Vicsek fractal lattice, and 'Tr' represents the trace of the Green's function matrix.

Using the above formalism, we have computed the DOS for the Vicsek fractal lattice in its different generations as depicted in Fig. 3. In general, for fractal lattices, the DOS display a multifractal character with the single-particle states are being localized following a power-law localization pattern [45–47]. This is what we observe in the DOS spectrum for the Vicsek fractal lattice model as shown in Fig. 3. As we are interested in the effect of the magnetic flux on the single-particle states in this fractal lattice, therefore we have illustrated the DOS for three different values of the magnetic flux, *viz.*, $\Phi = 0$, $\Phi_0/4$ and $\Phi_0/2$, respectively, for the first generation (\mathcal{G}_1)

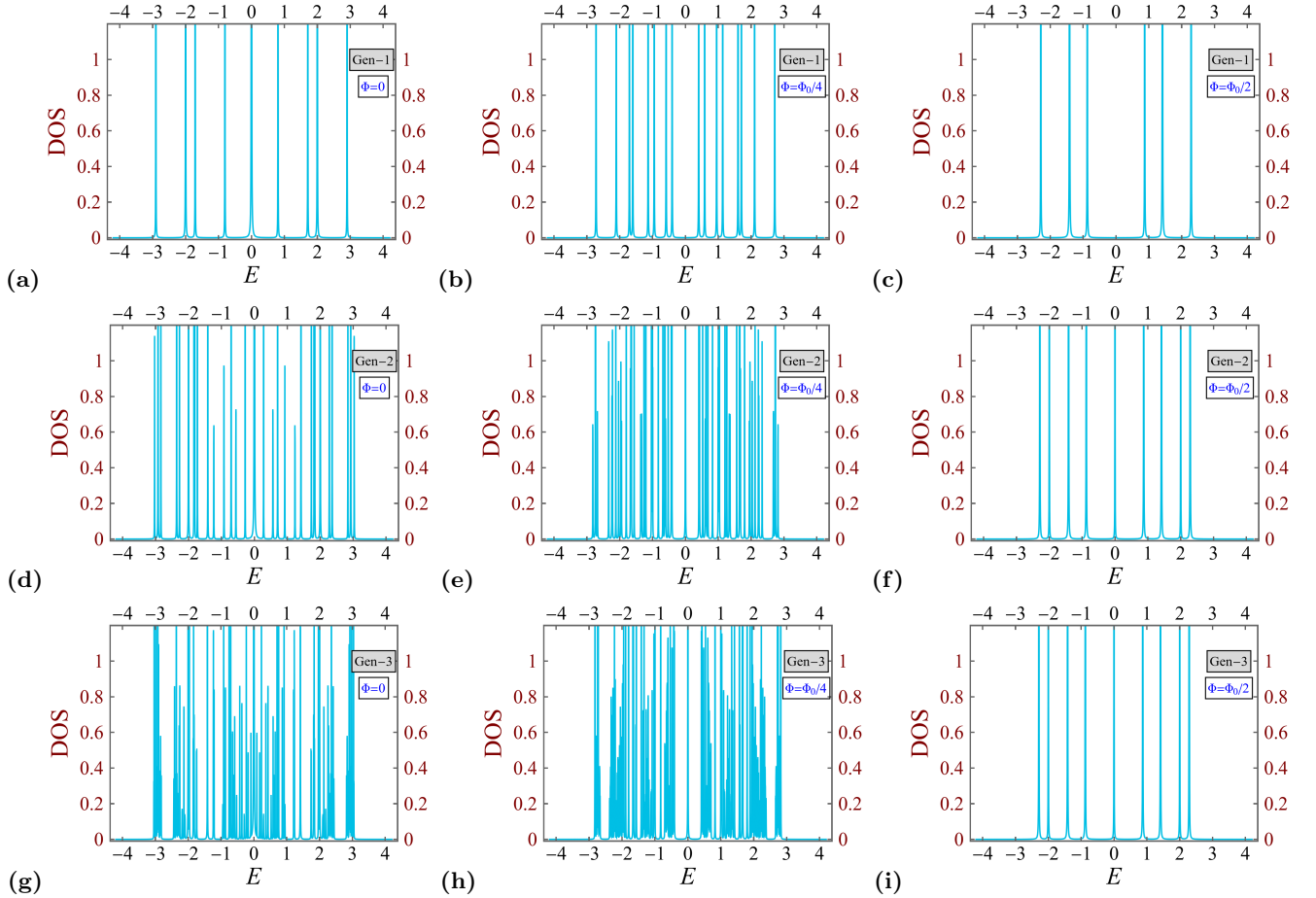


FIG. 3. The plots for the density of states (DOS) as a function of the energy (E) of the electron for the (a)-(c) first generation (\mathcal{G}_1), (d)-(f) second generation (\mathcal{G}_2), and (g)-(i) third generation (\mathcal{G}_3) Vicsek fractal lattice. The left column is for $\Phi = 0$, the middle column is for $\Phi = \Phi_0/4$, and the right column is for $\Phi = \Phi_0/2$.

[see Fig. 3(a)-(c)], second generation (\mathcal{G}_2) [see Fig. 3(d)-(f)], and third generation (\mathcal{G}_3) [see Fig. 3(g)-(i)] Vicsek fractal lattice. We note that, as the system size grows, we have more denser packing in the DOS spectrum as more number of states are available for the electron to occupy. However, if we focus on the extreme right column in Fig. 3, we observe that for $\Phi = \Phi_0/2$, the DOS spectrum for all the three generations \mathcal{G}_1 , \mathcal{G}_2 , and \mathcal{G}_3 , respectively, contracted to only a few sharp lines indicating towards the highly localized states. This clearly corroborates with the results for the energy spectrum depicted in the previous section and confirms the phenomenon of AB caging for this fractal lattice geometry.

In order to affirm our findings for the energy spectrum and the DOS, we have computed the two-terminal transmission probability of an electron through this fractal lattice system using the non-equilibrium Green's function (NEGF) technique [48–50]. To find out the transmission probability of an electron through our fractal system, we connect a finite size fractal system in between two semi-infinite leads, which are popularly known as the source (S) and drain (D). We send the electron into the fractal

system through the source and find the probability of it coming out of the system through the drain as we tune the value of magnetic flux in the system. The formula for the transmission probability is given by

$$T(E) = \text{Tr}[\mathbf{\Gamma}_S \mathbf{G}^r \mathbf{\Gamma}_D \mathbf{G}^a], \quad (4)$$

where \mathbf{G}^r and \mathbf{G}^a are the *retarded* and *advanced* Green's function matrices for the system (including the coupling to the semi-infinite leads) given by

$$\mathbf{G}^r = [\mathbf{E}I - \mathbf{H} - \Sigma_S^r - \Sigma_D^r]^{-1} \quad (5a)$$

$$\mathbf{G}^a = [\mathbf{E}I - \mathbf{H} - \Sigma_S^a - \Sigma_D^a]^{-1}, \quad (5b)$$

and $\mathbf{\Gamma}_S$ and $\mathbf{\Gamma}_D$ are the broadening or coupling matrices representing the coupling between the system and the leads, and they are mathematically defined as

$$\mathbf{\Gamma}_S = i(\Sigma_S^r - \Sigma_S^a) \quad (6a)$$

$$\mathbf{\Gamma}_D = i(\Sigma_D^r - \Sigma_D^a). \quad (6b)$$

$\Sigma_{S(D)}^r$ and $\Sigma_{S(D)}^a$ are the retarded and advanced self-energies associated with the two leads, *viz.*, the source

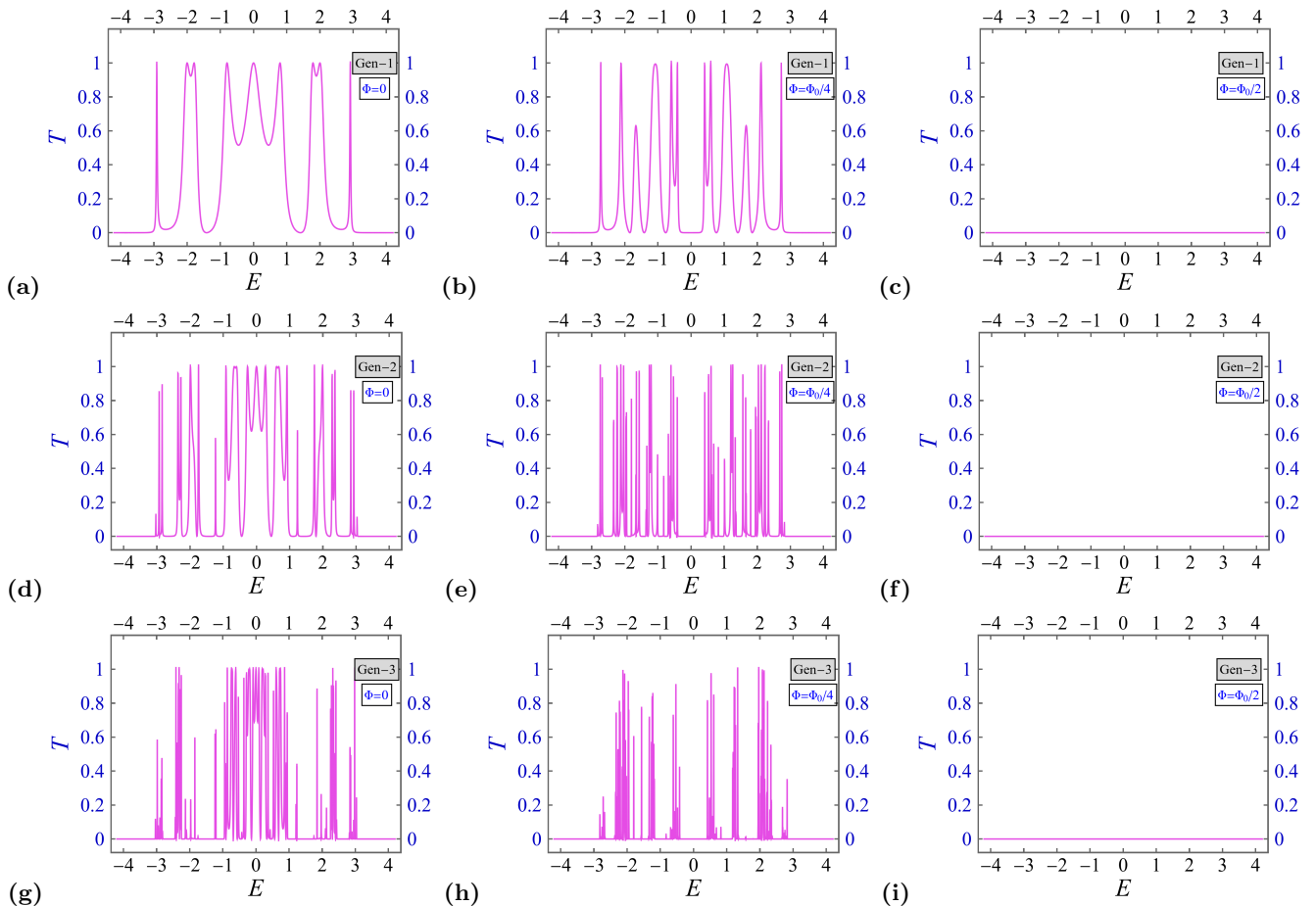


FIG. 4. The plots for the transmission probability (T) as a function of the energy (E) of the electron for the (a)-(c) first generation (\mathcal{G}_1), (d)-(f) second generation (\mathcal{G}_2), and (g)-(i) third generation (\mathcal{G}_3) Vicsek fractal lattice. The left column is for $\Phi = 0$, the middle column is for $\Phi = \Phi_0/4$, and the right column is for $\Phi = \Phi_0/2$.

and drain. The nonzero elements of the self-energy matrices are given by

$$\Sigma_S^r(p, p) = \frac{\tau_S^2}{2t_L^2} \left[(E - \varepsilon_L) - i\sqrt{4t_L^2 - (E - \varepsilon_L)^2} \right] \quad (7a)$$

$$\Sigma_D^r(q, q) = \frac{\tau_D^2}{2t_L^2} \left[(E - \varepsilon_L) - i\sqrt{4t_L^2 - (E - \varepsilon_L)^2} \right] \quad (7b)$$

$$\Sigma_S^a(p, p) = [\Sigma_S^r(p, p)]^\dagger \ \& \ \Sigma_D^a(q, q) = [\Sigma_D^r(q, q)]^\dagger \quad (7c)$$

where p and q denote the site numbers of the system with which the left lead (source) and right lead (drain) are connected, respectively. ε_L is the constant onsite potential for the atomic sites in the leads, t_L is the constant hopping integral between the neighboring sites in the leads, and $\tau_{S(D)}$ denote the coupling of the leads with the system. For our calculation, we set the parameters $\varepsilon_L = 0$, $t_L = 2$, and $\tau_{S(D)} = 1$.

Using the above prescription, we have calculated the transmission probability of an electron through the Vicsek fractal lattice for all the cases depicted in Fig. 3. We find that, for the cases $\Phi = 0$ (Fig. 4 left column)

and $\Phi = \Phi_0/4$ (Fig. 4 middle column), we get nonzero finite values of the transmission probability for an electron moving through the fractal system. The transmission probabilities show a lot of oscillations which is expected because of the fractal nature of the lattice system. However, our point of interest is $\Phi = \Phi_0/2$ (Fig. 4 right column). We find that, for the half flux quantum, *i.e.*, $\Phi = \Phi_0/2$, we get zero transmission probability of the electron for the entire energy range. It means that, at $\Phi = \Phi_0/2$, all the single-particle states in the system are *completely localized*. This quantifies and confirms our prediction of the AB caging phenomenon for this fractal geometry for a special value of the magnetic flux equal to half flux quantum. In Sec. IV, we discuss about the persistent current for the Vicsek fractal system, which in principle, could be measured in a real-life experiment.

Effect of onsite disorder on the AB caging phenomena: Before we end this section, let us briefly discuss the effect of the onsite disorder on the AB caging phenomena observed in a Vicsek fractal geometry. We will only focus on the case of half flux quantum, *i.e.*, $\Phi = \Phi_0/2$. We have calculated the DOS and the two-terminal trans-

port characteristics for this case with a random disorder in the onsite potential distribution $\varepsilon_n \sim [-\Delta/2, \Delta/2]$ of our system, where Δ is the width of the disorder strength. The results for the second generation fractal system are displayed in Fig. 5. We find that there is a broadening in the DOS spectrum (see Fig. 5(a)) which is resulted from the disorder distribution in the onsite potentials, however we still get zero transport (see Fig. 5(b)) through the system even in presence of this random onsite disorder distribution. Thus, we can conclude that the phenomenon of AB caging of an electron in a Vicsek fractal lattice is robust against the onsite disorder in the system. It is observed that, at $\Phi = \Phi_0/2$ (half flux quantum), the effective hopping amplitude between the two horizontal sites of a single diamond plaquette becomes zero. That is why, even with the introduction of onsite disorder in the system, the AB caging phenomenon persists and we still get the zero transmission probability for the electrons in the system. One can expect to get the similar result even for the off-diagonal (hopping) disorder because of same logic as explained above.

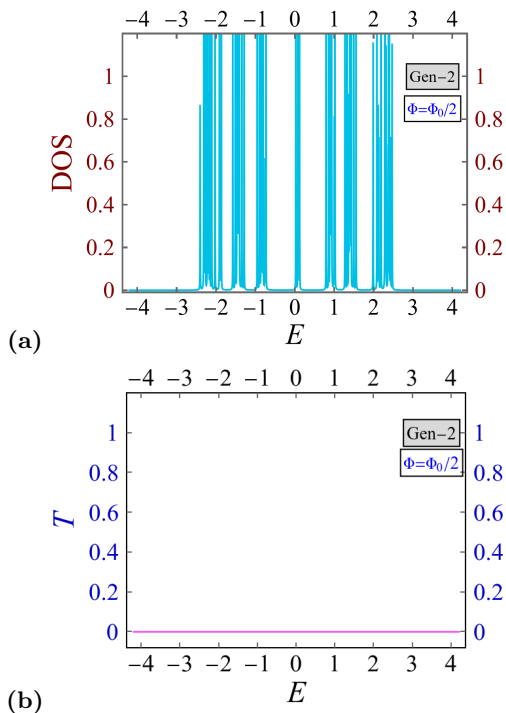


FIG. 5. The plots for the DOS and transmission probability (T) as a function of the energy (E) of the electron for the second generation Vicsek fractal lattice in presence of *random onsite disorder* of width $\Delta = 0.5$ in the system. We have chosen $\Phi = \Phi_0/2$.

IV. PERSISTENT CURRENT

It is important to quantify the AB caging phenomena in terms of some experimentally measurable quantity,

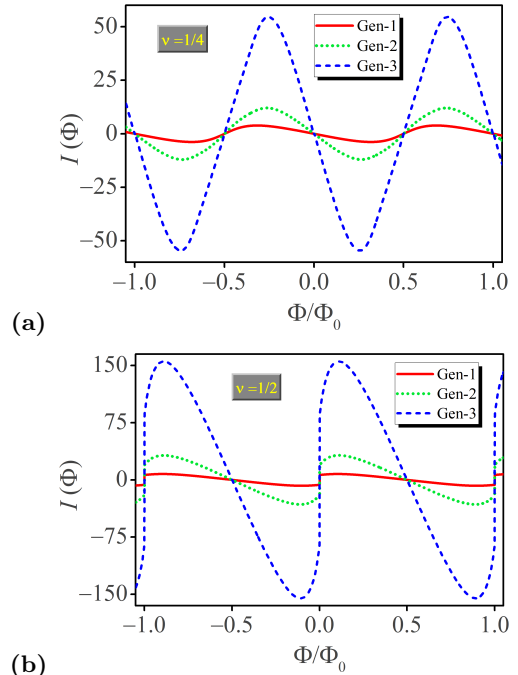


FIG. 6. Variation of the persistent current (I) as a function of the magnetic flux (Φ) in a Vicsek fractal lattice for (a) $\nu = 1/4$ filling and (b) $\nu = 1/2$ filling of the energy levels.

and the persistence current is a quantity which one can measure experimentally. Also, the study of the persistent current in this fractal system will give us a chance to explore the possibility of designing a quantum logic device using such a fractal system. Therefore, in this section, we discuss about the behavior of the persistent current in this closed-loop Vicsek fractal geometry. We remark that, it has no connection with the persistent current in the context of superconductivity. In our context, it is defined as a circulating current in a closed-loop geometry appearing because of the motion of an electron in the presence of a nonzero uniform magnetic flux in the system. The persistent current for the n th energy level in such closed-loop geometry at absolute zero temperature ($T = 0$ K) is given by [51–53]

$$\mathcal{I}_n = -\frac{\partial E_n}{\partial \Phi}. \quad (8)$$

Hence, the total persistent current in the fractal system is given by,

$$I(\Phi) = \sum_{n=1}^{\mathcal{N}_e} \mathcal{I}_n = -\sum_{n=1}^{\mathcal{N}_e} \frac{\partial E_n}{\partial \Phi}, \quad (9)$$

where \mathcal{N}_e is the number of spinless non-interacting electrons in the system. We define $\nu = \mathcal{N}_e/\mathcal{N}_\ell$ as the *filling factor* for an ℓ th generation Vicsek fractal system.

Using this formalism we have computed the persistent current in the Vicsek fractal lattice in its various generations for two different values of $\nu = 1/4$ and $1/2$ as

exhibited in Fig. 6(a) and (b), respectively. We note that, in both the cases, the persistent current increases as the system size increases. In fact, from these two plots, we are able to figure out a relationship between the persistent current in the ℓ th generation Vicsek fractal and $(\ell + 1)$ th generation Vicsek fractal as follows:

$$I_{\ell+1} = RI_{\ell}, \text{ with } R = 5 \text{ and } \ell \geq 1. \quad (10)$$

In Fig. 6, one can clearly identify that at $\Phi = \pm\Phi_0/2$, the persistent current vanishes in the system. Thus, this result corroborates with the phenomenon of AB caging for our fractal system and may be experimentally tested in the near future.

Before we conclude, it is worth mentioning that similar lattice model has been studied earlier [43] with a main focus to identify the staggered single-electron localization pattern in a Vicsek fractal geometry induced by the fractality of the lattice geometry in absence of any external magnetic flux. As compared to that, in the present study, our main focus is to understand the localization behavior, energy spectrum, transmission probability and persistent current in detail in a Vicsek fractal geometry as function of the magnetic flux. Secondly, in the earlier study, the real space renormalization group (RSRG) decimation method was used to obtain the results. In this method, some subtle features in the energy spectrum were missing because of the decimation of a certain set of sites. For example, in the present study, in Fig. 2, we find that a very robust flat band like energy eigenvalue appears in the energy spectrum at the energy $E = 0$ starting from the second-generation system onwards. This interesting feature was not identified in Ref. [43]. We have observed this in the present study, as here we have analyzed the energy spectrum using the exact diagonalization of the Hamiltonian matrices for different generation fractal lattice systems. Apart from that, in this work, we have quantified the AB caging phenomenon explicitly by calculating the transmission probability and the persistent current for various generations of the Vicsek fractal system. Additionally, we have also studied the effect of on-site disorder on the robustness of AB caging phenomena in such a fractal lattice.

V. CONCLUDING REMARKS

To conclude, we have demonstrated a mechanism by which one can completely block the mobility of an electron in a fractal geometry. Such caging of the electron happens for a special value of the underlying magnetic flux in the system and is governed by the geometrical structure of the basic building block of the corresponding fractal geometry. This intriguing phenomenon has been quantitatively verified by computation of the energy spectrum and the quantum transport for this fractal lattice model, and found to be robust against the on-site disorder in the system. Such controlled blocking of the quantum transport of an electron using an externally tunable magnetic flux could be very useful for the future quantum technology. For example, our results could be helpful in processing the quantum information in a quantum fractal system as well as for building efficient quantum algorithms using a quantum fractal network. In future, one can try to extend and generalize this idea of caging an electron in other possible closed-loop fractals.

ACKNOWLEDGMENTS

The author would like to thank Dr. Joydeep Majhi from IIT Bombay for some useful discussions during the course of this study.

CONFLICT OF INTEREST

The author declare no conflict of interest.

DATA AVAILABILITY STATEMENT

The data that support the findings of this study are available from the corresponding author upon reasonable request.

-
- [1] P. W. Anderson, *Phys. Rev.* **109**, 1492 (1958).
 - [2] E. Abrahams, P. W. Anderson, D. C. Licciardello, and T. V. Ramakrishnan, *Phys. Rev. Lett.* **42**, 673 (1979).
 - [3] B. Sutherland, *Phys. Rev. B* **34**, 5208 (1986).
 - [4] D. Leykam, A. Andreanov, and S. Flach, *Adv. Phys. X* **3**, 1473052 (2018).
 - [5] R. A. Vicencio Poblete, *Adv. Phys. X* **6**, 1878057 (2021).
 - [6] B. Pal, *Phys. Rev. B* **98**, 245116 (2018).
 - [7] B. Pal and G. Bouzerar, *J. Phys.: Condens. Matter* **37**, 135503 (2025).
 - [8] D. Bercioux, N. Goldman, and D. F. Urban, *Phys. Rev. A* **83**, 023609 (2011).
 - [9] J. Vidal, B. Douçot, R. Mosseri, and P. Butaud, *Phys. Rev. Lett.* **85**, 3906 (2000).
 - [10] A. Aharony, O. Entin-Wohlman, Y. Tokura, and S. Katsumoto, *Phys. Rev. B* **78**, 125328 (2008).
 - [11] A. Aharony, O. Entin-Wohlman, Y. Tokura, and S. Katsumoto, *Physica E* **42**, 629 (2010).
 - [12] J. Vidal, R. Mosseri, and B. Douçot, *Phys. Rev. Lett.* **81**, 5888 (1998).
 - [13] Y. Aharonov and D. Bohm, *Phys. Rev.* **115**, 485 (1959).
 - [14] S. Mukherjee, M. Di Liberto, P. Öhberg, R. R. Thomson, and N. Goldman, *Phys. Rev. Lett.* **121**, 075502 (2018).
 - [15] G. Cáceres-Aravena, D. Guzmán-Silva, I. Salinas, and R. A. Vicencio, *Phys. Rev. Lett.* **128**, 256602 (2022).

- [16] H. Li, Z. Dong, S. Longhi, Q. Liang, D. Xie, and B. Yan *Phys. Rev. Lett.* **129**, 220403 (2022).
- [17] A. Mukherjee, A. Nandy, S. Sil, and A. Chakrabarti, *J. Phys.: Condens. Matter* **33**, 035502 (2021).
- [18] A. M. Marques, J. Mögerle, G. Pelegrí, S. Flannigan, R. G. Dias, and A. J. Daley, *Phys. Rev. Res.* **5**, 023110 (2023).
- [19] M. Kremer, I. Petrides, E. Meyer, M. Heinrich, O. Zilberberg, and A. Szameit, *Nat. Commun.* **11**, 907 (2020).
- [20] M. Brzezińska, A. M. Cook, and T. Neupert, *Phys. Rev. B* **98**, 205116 (2018).
- [21] S. Pai and A. Prem, *Phys. Rev. B* **100**, 155135 (2019).
- [22] Z. F. Osseweijer, L. Eek, A. Moustaj, M. Fremling, and C. Morais Smith, *Phys. Rev. B* **110**, 245405 (2024).
- [23] L. Eek, Z. F. Osseweijer, and C. Morais Smith, [arXiv:2411.12341 \[cond-mat.mes-hall\]](https://arxiv.org/abs/2411.12341).
- [24] S. Manna, B. Pal, W. Wang, and A. E. B. Nielsen, *Phys. Rev. Res.* **2**, 023401 (2020).
- [25] A. A. Iliasov, M. I. Katsnelson, and S. Yuan, *Phys. Rev. B* **101**, 045413 (2020).
- [26] M. Fremling, M. van Hooft, C. M. Smith, and L. Fritz, *Phys. Rev. Res.* **2**, 013044 (2020).
- [27] B. Pal and K. Saha, *Phys. Rev. B* **97**, 195101 (2018).
- [28] A. Nandy, *Phys. Scr.* **96**, 045802 (2021).
- [29] H. Hanafi, P. Menz, and C. Denz, *Adv. Optical Mater.* **10**, 2102523 (2022).
- [30] Y. Xie, L. Song, W. Yan, S. Xia, L. Tang, D. Song, J.-W. Rhim, and Z. Chen, *APL Photonics* **6**, 116104 (2021).
- [31] L. Song, Y. Xie, S. Xia, L. Tang, D. Song, J.-W. Rhim, and Z. Chen, *Laser Photonics Rev.* **17**, 2200315 (2023).
- [32] S. Biswas and A. Chakrabarti, *Physica E* **153**, 115762 (2023).
- [33] G. Koch and A. Posazhennikova, *Phys. Rev. A* **110**, 033301 (2024).
- [34] M. Amundsen, V. Juričić, and J. A. Ouassou, *Appl. Phys. Lett.* **125**, 092601 (2024).
- [35] X. Zhang, N. Li, G.-C. Gu, H. Wang, D. Nieckarz, P. Szabelski, Y. He, Y. Wang, C. Xie, Z.-Y. Shen, J.-T. Lü, H. Tang, L.-M. Peng, S.-M. Hou, K. Wu, and Y.-F. Wang, *ACS Nano* **9**, 11909 (2015).
- [36] J. Shang, Y. Wang, M. Chen, J. Dai, X. Zhou, J. Kuttner, G. Hilt, X. Shao, J. M. Gottfried, and K. Wu, *Nat. Chem.* **7**, 389 (2015).
- [37] S. N. Kempkes, M. R. Slot, S. E. Freeney, S. J. M. Zevenhuizen, D. Vanmaekelbergh, I. Swart, and C. M. Smith, *Nat. Phys.* **15**, 127 (2019).
- [38] R. Canyellas, C. Liu, R. Arouca, L. Eek, G. Wang, Y. Yin, D. Guan, Y. Li, S. Wang, H. Zheng, C. Liu, J. Jia, and C. Morais Smith, *Nat. Phys.* **20**, 1421 (2024).
- [39] D. Bercioux and A. Iñiguez, *Nat. Phys.* **15**, 111 (2019).
- [40] X. Pan, Z. Wei, and T. Che, *Aerosp. Sci. Technol.* **153**, 109429 (2024).
- [41] H. Gopalakrishnan and S. Anurag Prasad, *Chaos Solitons Fractals* **181**, 114607 (2024).
- [42] F. Ma, X. Wang, P. Wang and X. Luo, *Europhys. Lett.* **133**, 40004 (2021).
- [43] B. Pal and A. Chakrabarti, *Phys. Rev. B* **85**, 214203 (2012).
- [44] B. Pal, P. Patra, J. P. Saha, and A. Chakrabarti, *Phys. Rev. A* **87**, 023814 (2013).
- [45] A. Chakrabarti, *Phys. Rev. B* **72**, 134207 (2005).
- [46] B. Pal and A. Chakrabarti, *Eur. Phys. J. B* **85**, 307 (2012).
- [47] A. Nandy, B. Pal, and A. Chakrabarti, *J. Phys.: Condens. Matter* **27**, 125501 (2015).
- [48] S. Datta, *Electronic Transport in Mesoscopic Systems*, Cambridge University Press, Cambridge, 1995.
- [49] S. Datta, *Quantum Transport: Atom to Transistor*, Cambridge University Press, Cambridge, 2005.
- [50] M. Dey, S. K. Maiti, and S. N. Karmakar, *Org. Electron.* **12**, 1017 (2011).
- [51] H.-F. Cheung, E. K. Riedel, and Y. Gefen, *Phys. Rev. Lett.* **62**, 587 (1989).
- [52] S. K. Maiti and A. Chakrabarti, *Phys. Rev. B* **82**, 184201 (2010).
- [53] B. Pal, *J. Appl. Phys.* **137**, 144301 (2025).